In situ construction of heterostructured bimetallic sulfide/phosphide with rich interfaces for high-performance aqueous Zn-ion batteries

Fang Yang[a], Yuenian Shen[b], Ze Cen [a], Jie Wan [a], Shijie Li[*c], Guanjie He[d], Junqing Hu[b,e] and Kaibing Xu[*b]

[a] School of Mechanical and Automotive Engineering, Shanghai University of Engineering Science, Shanghai, 201620, China

[b] State Key Laboratory for Modification of Chemical Fibers and Polymer Materials, Research Center for Analysis and Measurement & College of Materials Science and Engineering, Donghua University, Shanghai, 201620, China

[c] Institute of Innovation & Application, National Engineering Research Center for Marine Aquaculture, Zhejiang Ocean University, Zhoushan, Zhejiang Province, 316022, China

[d] School of Chemistry, University of Lincoln, Brayford Pool, Lincoln LN6 7TS, UK

[e] College of Health Science and Environmental Engineering, Shenzhen Technology University, Shenzhen 518118, China

E-mail address: lishijie@zjou.edu.cn (S. Li), xukaibing@dhu.edu.cn (K. Xu).

Abstract: It is still challenging to develop suitable cathode structures for high rate and stable aqueous Zn-ion batteries. Herein, a phosphating-assisted interfacial engineering strategy is designed for the controllable conversion of $NiCo_2S_4$ nanosheets into heterostructured NiCoP/$NiCo_2S_4$ as the cathodes in aqueous Zn-ion batteries. The multicomponent heterostructures with rich interfaces can not only improved electrical conductivity but also enhanced diffusion pathways for Zn-ion storage. As expected, the NiCoP/$NiCo_2S_4$ electrode have a high performance with large specific capacity of 251.1 mA h g^{-1} at a high current density of 10 A g^{-1} and excellent rate capability (retaining about 76% even at 50 A g^{-1}). Accordingly, the Zn-ion battery using NiCoP/$NiCo_2S_4$ as the cathode delivers a high specific capacity (265.1 mA h g^{-1} at 5 A g^{-1}), a long-term cycling stability (96.9% retention after 5000 cycles), and a competitive energy density (444.7 W h kg^{-1} at the power density of 8.4 kW kg^{-1}). This work therefore provides a simple phosphating-assisted interfacial engineering strategy for construct heterostructured electrode materials with rich interfaces for the development of high-performance energy storage devices in the future.

Key words: Phosphating; Heterostructure; NiCoP/$NiCo_2S_4$; Zn-ion batteries; High capacity

1. Introduction

To alleviate the excessive consumption of traditional fossil fuels and increasing environmental pollution issues, it is particularly urgent and important to develop high-efficient and clean energy storage devices. Typically, lithium (Li)-ion batteries have been widely used for a variety of energy storage systems, such as portable electronics, electric vehicles, and grid-scale energy-storage systems [1]. However, the large-scale application of Li-ion batteries is still a huge challenge because of limited lithium resources and toxic organic electrolytes [2-5]. Recently, researchers have focused on the exploration of high performance aqueous rechargeable batteries with low cost and reliable safety [6-10]. Among various rechargeable batteries, aqueous Zn-ion batteries are emerging as one of the most competitive candidates to replace Li-ion batteries by virtue of its high theoretical capacity of the zinc anode (820 mAh g^{-1}), high working voltage (~1.8 V), as well as its low cost and low toxicity [11-20]. However, the unsatisfactory energy/power density and poor cycling stability severely limit its practical application. Designing and constructing highly active cathode materials have been demonstrated as a promising strategy to improve the performance of Zn-ion batteries.

Transition metal sulfides have been extensively investigated as electrode materials due to its higher electronic conductivity and better reversible electrochemical properties than their oxide counterparts [21-24]. Especially, $NiCo_2S_4$ electrode materials have been proved to have better electronic conductivities of about 100 times higher than that of $NiCo_2O_4$ [21, 25]. In addition, compared to its

corresponding single-component sulphides (NiS_x and CoS_x), $NiCo_2S_4$ have significantly richer redox reactions because of multiple available oxidation states and faster electron transfer properties [26, 27]. For instance, Han et al. developed sulfur-deficient $NiCo_2S_{4-x}$ nanotube arrays on carbon cloth as an effective cathode material for flexible Zn batteries, which delivered a high capacity of 298.3 mAh g^{-1} at 0.5 A g^{-1} and superior rate capability [28]. On the other hand, transition metal phosphides have attracted extensive research interests due to their unique electronic structure and high thermal/chemical stability, which show high electrocatalytic activity/durability and good conductivity [29-33]. For example, Zhang et al. developed ultrafine and highly active bimetallic $Co_xNi_{1-x}P$ nanoparticle loaded on carbon nanofibers, exhibiting an extraordinary specific capacitance of 3514 F g^{-1} at 5 A g^{-1}[34]. Therefore, the in-situ construction of metal phosphides based on metal sulfides can effectively realize the coupling of their respective advantages. Moreover, novel multicomponent heterostructures formed by metal sulfides and phosphides with rich interfaces is emerging as an effective strategy to generate abundant interfaces for fast charge transfer and improve the number of highly-exposed active sites for redox reactions, showing great application potential.

In this work, we have developed a controllable route to fabricate heterostructured NiCoP/$NiCo_2S_4$ nanosheet arrays on carbon cloth. The heterostructured NiCoP/$NiCo_2S_4$ electrode shows the strong synergistic effect and rich interfaces between NiCoP and $NiCo_2S_4$, and delivers a high specific capacity of 251.1 mA h g^{-1} at a high current density of 10 A g^{-1} and excellent rate capability. In the constructed

aqueous Zn-ion battery, the NiCoP/$NiCo_2S_4$//Zn battery is able to deliver a high specific capacity of 265.1 mA h g^{-1} at 5 A g^{-1} and the good cycling stability (capacity retention of 96.9% after 5000 cycles). Most importantly, this battery offers a high energy density of 444.7 W h kg^{-1} at the power density of 8.4 kW kg^{-1}. It is therefore significant to establish transition metal sulfides and phosphides heterostructured materials for enhancing the energy storage performance as the cathodes in aqueous Zn-ion batteries.

2. Experimental

2.1 Synthesis of $NiCo_2S_4$ nanosheet arrays

Firstly, $Ni(NO_3)_2·6H_2O$ (1 mmol), $Co(NO_3)_2·6H_2O$ (2 mmol), and hexamethylenetetramine (5.7 mmol) were dissolved in deionized water (25 mL) and ethanol (25 mL) under vigorous stirring. The resulting pink solution was then transferred into a 60 mL stainless steel autoclave with a piece of pretreated carbon cloth (1 × 4 cm^2) and kept sealed at 95 ℃ for 8 h. Subsequently, the obtained precursor on carbon cloth was annealed in air at 350 ℃ for 2 h. Finally, the above carbon cloth was immersed in the 50 mL deionized water with 1 g of $Na_2S·9H_2O$, and maintained at 100 ℃ for 24 h to obtain $NiCo_2S_4$ samples.

2.2 Synthesis of NiCoP/$NiCo_2S_4$ nanosheet arrays

To fabricate the NiCoP/$NiCo_2S_4$ nanosheet arrays, the $NiCo_2S_4$ nanosheet arrays on carbon cloth were annealed with the presence of NaH_2PO_2 (0.25−1 g) under N_2 atmosphere at 350−450 ℃ for 1−4 h. The mass loadings of $NiCo_2S_4$ and

$NiCoP/NiCo_2S_4$ materials were 0.60 and 0.63 mg cm^{-2}, respectively. For comparison, the $NiCo_2O_4$ nanosheet arrays were prepared under 400 ℃ for 2 h with 0.5 g NaH_2PO_2 to obtain NiCoP nanosheet arrays.

2.3 Materials characterization

The as-obtained materials were investigated by scanning electron microscopy (SEM; Hitachi, S-4800), transmission electron microscopy (TEM; JEOL, JEM-2100F), X-ray diffractometer (XRD; Rigaku, D/max-2550 PC), X-ray photoelectron spectroscopy (XPS; Thermo Fisher, Escalab 250Xi), and Brunauer-Emmett-Teller analyzer (BET; Quantachrome, Autosorb-iQ).

2.4 Electrochemical measurement

The electrochemical measurements were carried out on an electrochemical workstation (Metrohm Autolab PGSTAT302N, the Netherlands). A three-electrode system was performed for the evaluation of electrochemical properties of individual electrodes in 1 M KOH aqueous solution. The $NiCoP/NiCo_2S_4$ nanosheet arrays on carbon cloth was used directly as the working electrode, the saturated calomel electrode as a reference, and a platinum plate as the counter electrode. The aqueous Zn-ion battery was assembled using $NiCoP/NiCo_2S_4$ materials as the cathode and a piece of commercial Zn plate as the anode with the mixed solution of 1 M KOH and 0.01 M $Zn(CH_3COO)_2$, and two-electrode configuration was carried out to assess the electrochemical performance of the as-fabricated batteries.

3. Results and discussion

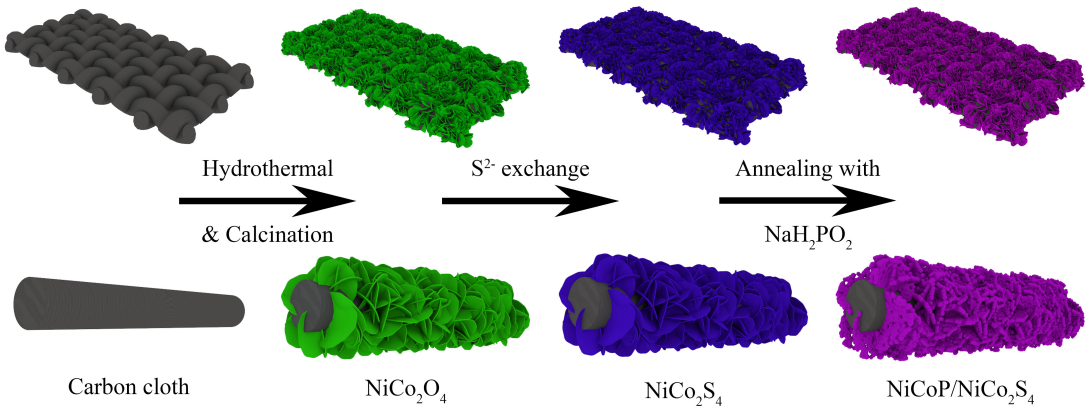

Fig. 1 Schematic illustration of the heterostructured NiCoP/$NiCo_2S_4$ nanosheet arrays supported on the carbon cloth.

Fig. 1 schematically illustrates the entire preparation procedures of heterostructured NiCoP/$NiCo_2S_4$ nanosheet arrays on carbon cloth. First of all, $NiCo_2O_4$ nanosheets are directly grown on the bare carbon cloth through a facile hydrothermal reaction, and calcined under air atmosphere to improve their crystallinity. After that, hydrothermal reaction is once again employed to realize the phase transformation between $NiCo_2O_4$ and $NiCo_2S_4$ samples by using $Na_2S·9H_2O$ as the sulfur source, where all the O^{2-} is exchanged into S^{2-} by Kirkendall effect. Finally, to accomplish the interfacial engineering of $NiCo_2S_4$ samples, phosphate treatment is conducted with NaH_2PO_2 as the phosphorus source. During this process, newly-formed NiCoP nanoparticles are embedded into $NiCo_2S_4$ nanosheets, generating an updated heterostructured nanostructure with rich interfaces due to the higher electronegativity of P than Ni and Co [35]. The NiCoP/$NiCo_2S_4$ electrode prepared under 400 ℃ for 2 h with 0.5 g of NaH_2PO_2 is discussed in the following sections, unless otherwise

stated, as it shows the highest specific capacities.

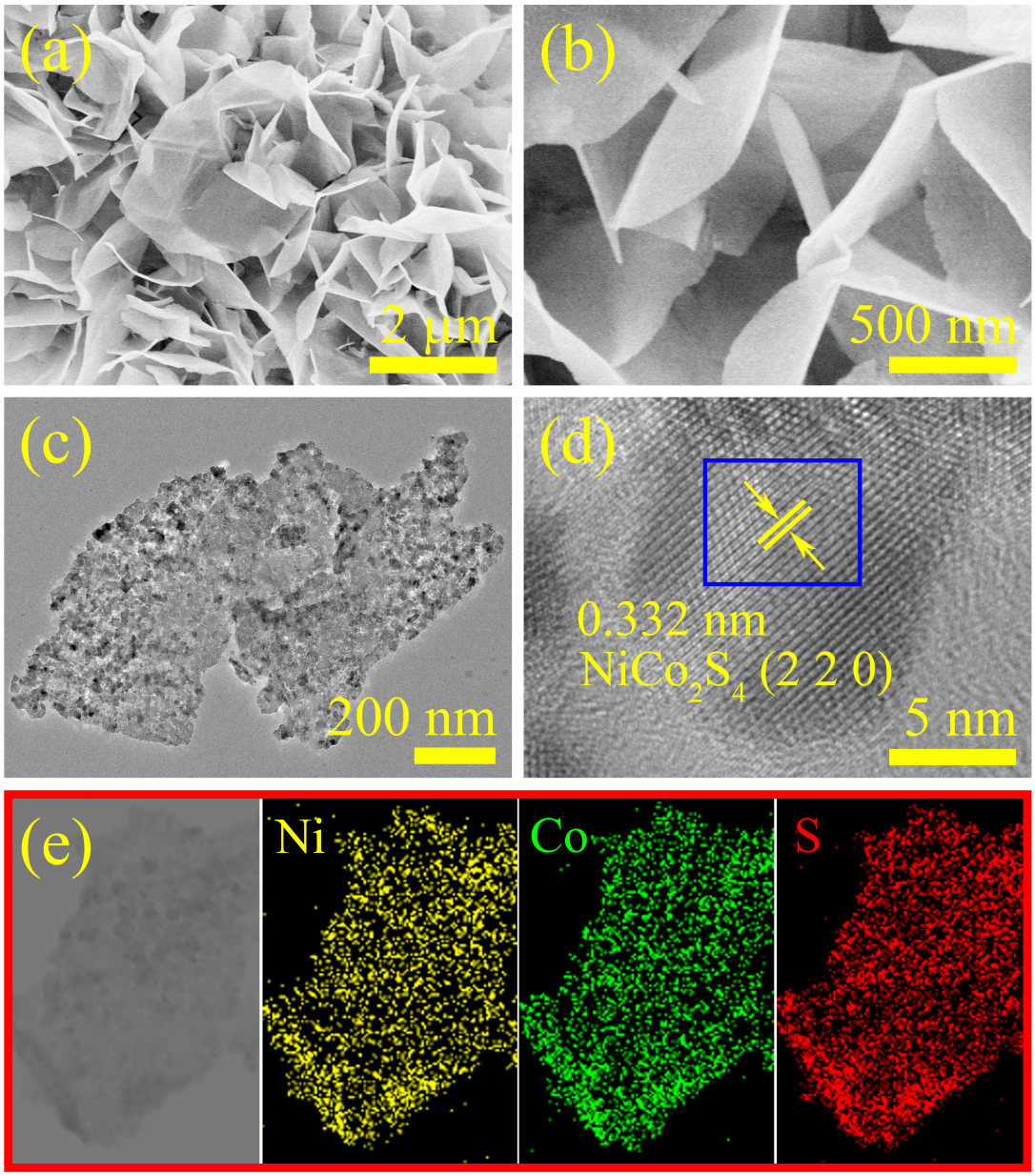

Fig. 2 (**a**, **b**) SEM, (**c**) TEM, (**d**) HRTEM, (**e**) elemental mapping images of $NiCo_2S_4$ nanosheets.

The micromorphology of $NiCo_2S_4$ nanosheets on carbon cloth was preliminarily investigated by scanning electron microscopy (SEM) and transmission electron microscopy (TEM) (**Fig. 2**). The SEM images, **Fig. 2a** and **b**, show that $NiCo_2S_4$

nanosheets derived from $NiCo_2O_4$ nanosheets (**Fig. S1**) remain uniformly supported on the carbon cloth, and these nanosheets are interconnected to each other. The TEM image of $NiCo_2S_4$ nanosheet is presented in **Fig. 2c**, it can be distinctly seen that numerous small pores are uniformly distributed throughout the whole surface. The high-resolution TEM image (HRTEM) characterization clearly displays the lattice fringes with an interplanar distance of 0.332 nm, corresponding well to the (220) plane of $NiCo_2S_4$ lattice (**Fig. 2d**). Furthermore, the energy dispersive X-ray spectroscopy (EDS) element mapping images, **Fig. 2e**, directly show the even distribution of Ni, Co and S elements in the $NiCo_2S_4$ nanosheet.

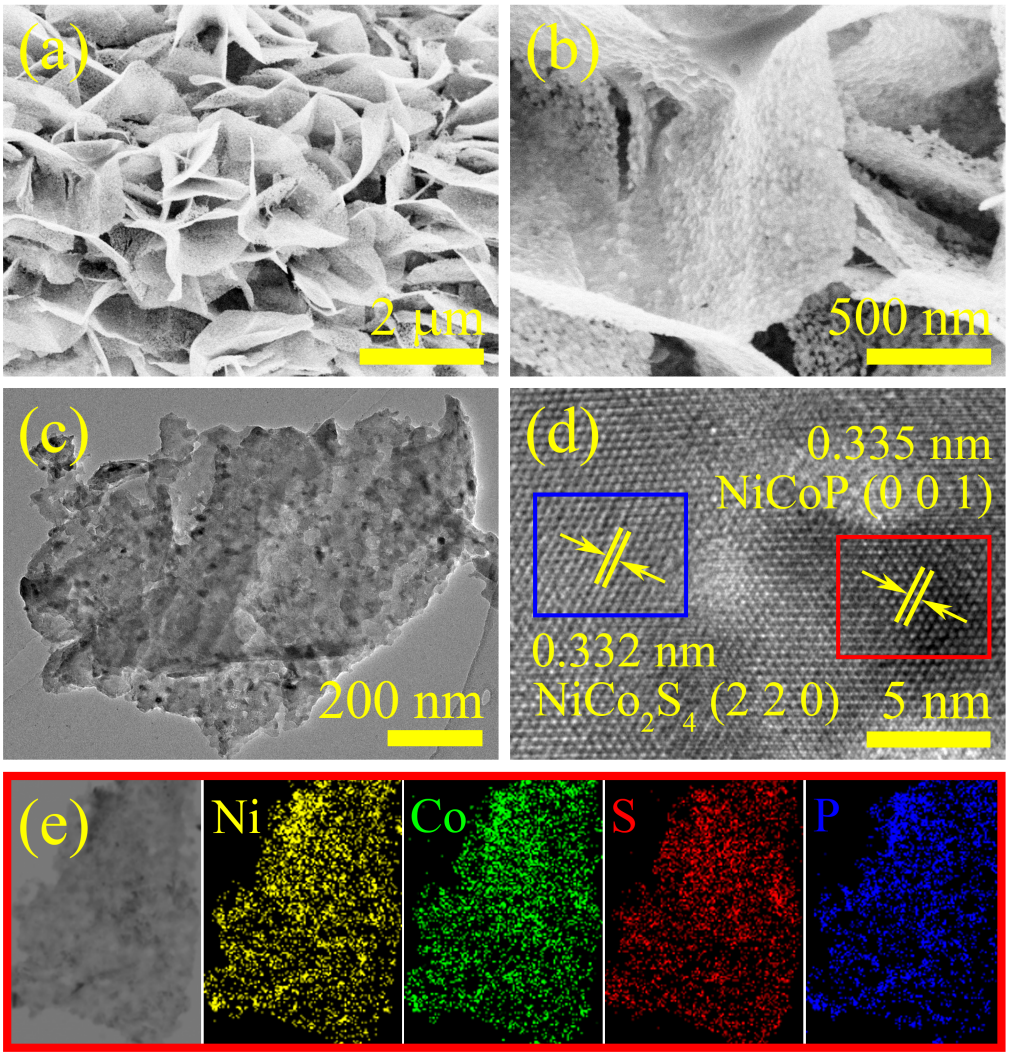

Fig. 3 (**a**, **b**) SEM, (c) TEM, (**d**) HRTEM, and (**e**) the corresponding elemental mapping images of NiCoP/$NiCo_2S_4$ nanosheets.

According to the SEM images of **Fig. 3a** and **b**, the densely packed and highly ordered NiCoP/$NiCo_2S_4$ nanosheet arrays are uniformly grown on carbon cloth surface, and these nanosheets are interconnected and intersected with each other with plenty of spaces, which are beneficial to the charge transportation and ion diffusion, thus enhancing the specific capacity. Compared with $NiCo_2S_4$ nanosheets, the surface of well-kept $NiCo_2S_4$ nanosheets becomes much rougher after phosphating treatment due to the formation of NiCoP nanoparticles. Moreover, the effects of phosphating conditions on the morphology of NiCoP/$NiCo_2S_4$ materials are also systematically investigated by adjusting the treatment temperature, the reaction time and the mass of NaH_2PO_2. As shown in **Fig. S2**, with the increase of temperature, time and amount of the P source, more NiCoP nanoparticles are generated on the $NiCo_2S_4$ nanosheets. Additionally, the Brunauer-Emmett-Teller (BET) surface areas were also tested (**Fig. S3**). The specific area of NiCoP/$NiCo_2S_4$ is 26.2 $m^2\ g^{-1}$, while that of $NiCo_2S_4$ is 27.3 $m^2\ g^{-1}$. The decrease in specific surface area may be caused by the newly-formed NiCoP nanoparticles plugging the pores in the $NiCo_2S_4$ nanosheets. The formation of heterostructured NiCoP/$NiCo_2S_4$ nanosheets is further confirmed by TEM, as shown in **Fig. 3c**, NiCoP nanoparticles are distributed on the surface of $NiCo_2S_4$ nanosheets, which is consistent with the result from SEM analysis. **Fig. 3d** shows the HRTEM of NiCoP/$NiCo_2S_4$ nanosheet, the obvious lattice fringes spaced at 0.332 nm and 0.335

nm, corresponding well to the (220) plane of $NiCo_2S_4$ and (001) plane of NiCoP. The EDS mapping images (**Fig. 3e**) also confirm that Ni, Co, S and P elements are uniformly distributed throughout the $NiCoP/NiCo_2S_4$ nanosheet.

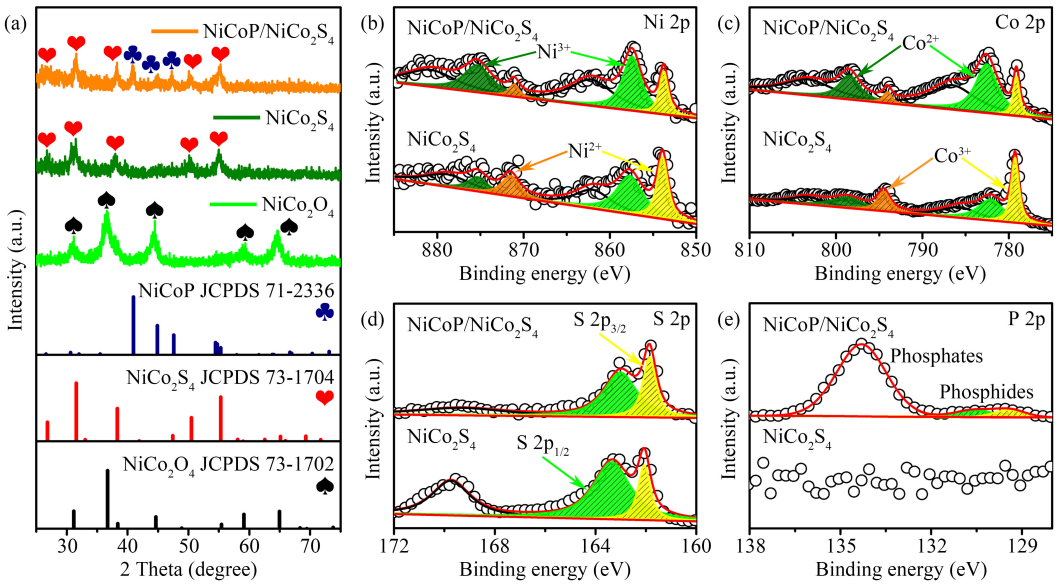

Fig. 4 (**a**) XRD patterns of $NiCo_2O_4$, $NiCo_2S_4$ and $NiCoP/NiCo_2S_4$ samples. (**b**) Ni 2p, (**c**) Co 2p, (**d**) S 2p and (**e**) P 2p core-level XPS spectra of $NiCo_2S_4$ and $NiCoP/NiCo_2S_4$ samples.

The phase of as-prepared materials was firstly acquired through the analysis of X-ray diffraction (XRD) data. As shown in **Fig. 4a**, the XRD pattern of $NiCoP/NiCo_2S_4$ samples display well-defined diffraction peaks, which are well matched with the standard XRD patterns of $NiCo_2S_4$ (JCPDS No. 73-1704) and NiCoP (JCPDS No. 71-2336), confirming the coexistence of NiCoP and $NiCo_2S_4$ after phosphating treatment without any residues or contaminants. Moreover, X-ray photoelectron spectroscopy (XPS) is further performed to investigate elemental compositions and

valence states of NiCoP/$NiCo_2S_4$ samples. As shown in **Fig. S4a**, there is an extra P signal in NiCoP/$NiCo_2S_4$ sample compared to the original $NiCo_2S_4$ sample. In the Ni 2p region (**Fig. 4b**), the spin orbital located at 875.4 and 857.4 eV stands for the presence of Ni^{3+}, while another one centered at 871.1 and 853.8 eV proves the existence of Ni^{2+} [36, 37]. In the case of Co 2p spectrum (**Fig. 4c**), two strong peaks located at the binding energy of 798.5 and 782.6 eV stands for the presence of Co^{2+}, and the other two peaks at 794.0 and 779.1 eV prove the existence of Co^{3+} [38, 39]. Therefore, the chemical composition of as-prepared materials contain the cations of Ni^{2+}, Ni^{3+}, Co^{2+}, and Co^{3+}. As for S 2p spectrum (**Fig. 4d**), apart from the shake-up satellite peaks at 169.3 eV, two signal peaks are located at 163.0 eV for S $2p_{1/2}$ and 161.8 eV for S $2p_{3/2}$, corresponding well to metal-sulfur (M-S) bonds in the samples [40, 41]. In the P 2p region (**Fig. 4e**), the dominant peak located at 134.3 eV represents that P exists mainly in the form of phosphate ions. And two signal peaks at 130.6 and 129.4 eV correspond to P $2p_{1/2}$ and P $2p_{3/2}$ spin orbitals [42, 43], corresponding well to metal phosphides. On the other hand, there is no signal in the P 2p region for pure $NiCo_2S_4$ sample. These results suggest that the heterostructured NiCoP/$NiCo_2S_4$ electrodes have been successfully prepared through the phosphate treatment by the NaH_2PO_2 as phosphorus source.

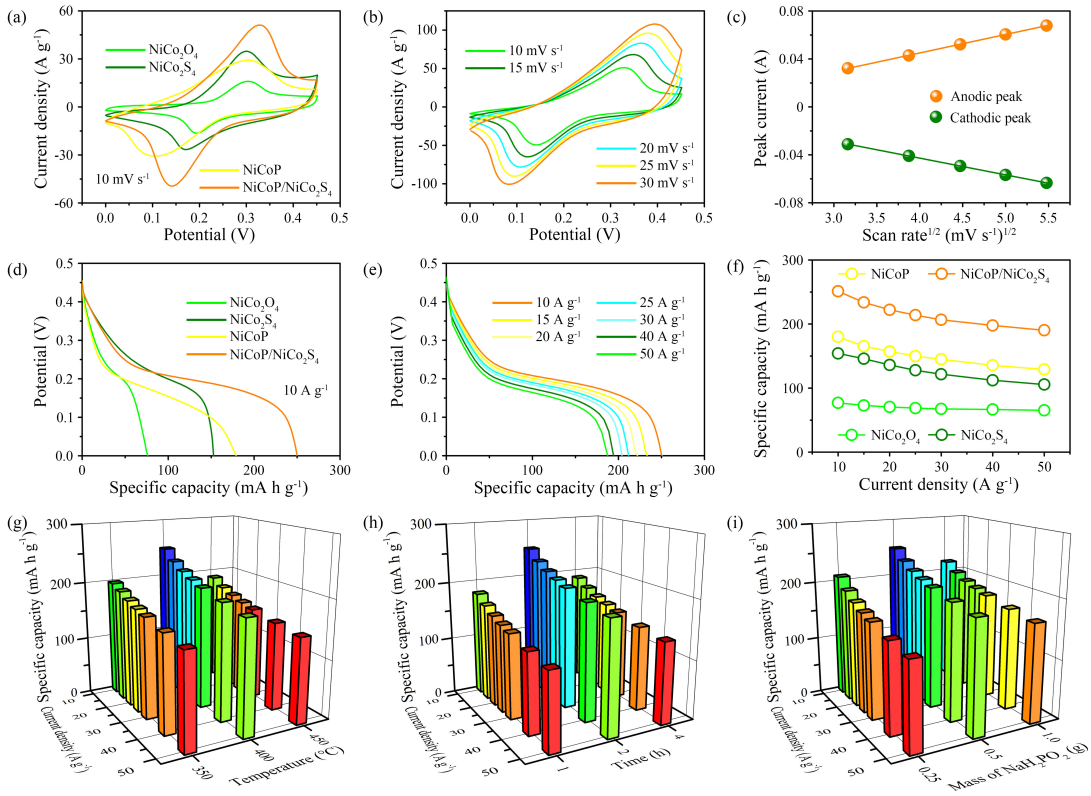

Fig. 5 Comparison of (**a**) CV and (d) discharge curves of $NiCo_2O_4$, $NiCo_2S_4$, NiCoP and NiCoP/$NiCo_2S_4$ electrodes. (**b**) CV and (**e**) discharge curves of NiCoP/$NiCo_2S_4$ electrode. (**c**) Variation in the redox peak currents with the square root of the scan rates of NiCoP/$NiCo_2S_4$ electrode. (**f**) Specific capacities versus current densities of $NiCo_2O_4$, $NiCo_2S_4$, NiCoP and NiCoP/$NiCo_2S_4$ electrodes. Specific capacities of NiCoP/$NiCo_2S_4$ electrodes as a function of (**g**) phosphating temperature, (**h**) reaction time and (**i**) mass of NaH_2PO_2.

The electrochemical performances of as-prepared samples were conducted on the three-electrode system with 1 M KOH as the electrolyte. **Fig. 5a** shows the comparison cyclic voltammetry (CV) curves of $NiCo_2O_4$, $NiCo_2S_4$, NiCoP and NiCoP/$NiCo_2S_4$ electrodes at the same scan rate of 10 mV s^{-1}. The current density and

integral area of NiCoP/$NiCo_2S_4$ are much higher than that of $NiCo_2O_4$, $NiCo_2S_4$, and NiCoP electrodes, suggesting the enhanced specific capacity and faster redox reaction kinetics. As the scan rates increase from 10 to 30 mV s^{-1}, the CV curves of NiCoP/$NiCo_2S_4$ electrode remain symmetric redox peaks (**Fig. 5b**), indicating the great reversibility of redox reactions. As shown in **Fig. 5c**, there is near linear relationship between peak currents and the square root of scan rates, demonstrating that the redox reactions for NiCoP/$NiCo_2S_4$ electrode are diffusion-controlled [3, 36]. The improved specific capacity can also be achieved through the analysis of discharge curves, as depicted in **Fig. 5d**, where the discharge plateau of NiCoP/$NiCo_2S_4$ electrode is much longer than others at the same current density of 10 A g^{-1}. Additionally, in contrast to $NiCo_2O_4$, $NiCo_2S_4$, and NiCoP electrodes, the discharge curves of the heterostructured NiCoP/$NiCo_2S_4$ remain steady discharge plateau as the current densities increase from 10 to 50 A g^{-1}, indicating the good rate performance (**Fig. 5e** and **Fig. S5**). The highest specific capacity obtained for the NiCoP/$NiCo_2S_4$ electrode is 251.1 mA h g^{-1} at a high current density of 10 A g^{-1} (**Fig. 5f**), which is higher than that of $NiCo_2O_4$ (76.9 mA h g^{-1}), $NiCo_2S_4$ (154.2 mA h g^{-1}) and NiCoP (180.0 mA h g^{-1}). Importantly, the NiCoP/$NiCo_2S_4$ electrode exhibits exceptional capacitive retention at a high current density. Even after increasing the current density to 50 A g^{-1}, the NiCoP/$NiCo_2S_4$ electrode shows capacity of 190.3 mA h g^{-1}, which is about 76% retention of that at 10 A g^{-1}. The specific capacity of NiCoP/$NiCo_2S_4$ is close or even superior to many similar works, such as Co_3S_4 (234.0 mA h g^{-1} at 8 A g^{-1}) [8], R-Co_3O_4 (212.6 mA h g^{-1} at 2 mA cm^{-2}) [18], Ni_3S_2@PANI (247.6 mA h g^{-1}

at 11.4 A g^{-1}) [44], and $NiCo_2O_4$ (183.1 mA h g^{-1} at 1.6 A g^{-1}) [45]. **Fig. 5g-i**, **Fig. S6**, and **Fig. S7** show the electrochemical performances of the NiCoP/$NiCo_2S_4$ electrode under different phosphating conditions, it makes clear that the optimal condition for NiCoP/$NiCo_2S_4$ electrode is 400 °C for 2 h with 0.5 g NaH_2PO_2, which contributes to the highest specific capacity.

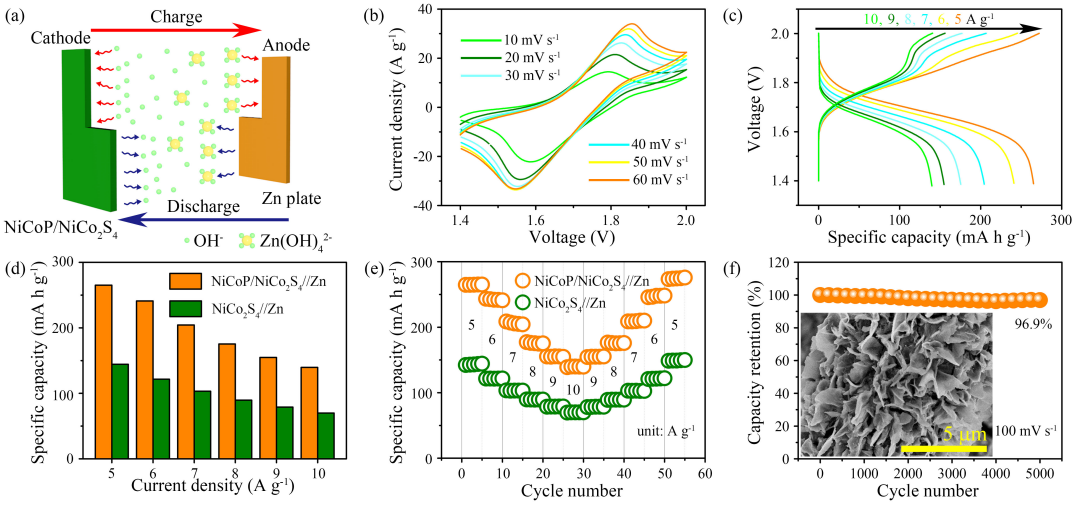

Fig. 6 (**a**) Schematic diagram of reaction mechanism of NiCoP/$NiCo_2S_4$//Zn battery. (**b**) CV and (**c**) charge-discharge curves of NiCoP/$NiCo_2S_4$//Zn battery. (**d**) Specific capacities versus current densities and (**e**) rate performances of $NiCo_2S_4$//Zn and NiCoP/$NiCo_2S_4$//Zn batteries. (**f**) Cycling test of NiCoP/$NiCo_2S_4$//Zn battery and SEM image of NiCoP/$NiCo_2S_4$ cathode after 5000 cycles (inset).

The outstanding specific capacity and high rate capability of the heterostructured NiCoP/$NiCo_2S_4$ electrode deliver a great potential as advanced cathodes in aqueous Zn-ion battery. An aqueous Zn-ion battery is assembled by using NiCoP/$NiCo_2S_4$ electrode as the cathode and Zn plate as the anode with the mixed solution of 1 M

KOH and 0.01 M $Zn(CH_3COO)_2$. The NiCoP/$NiCo_2S_4$ reacts with OH^- on the cathode, when reversible $Zn(OH)^{2-}/Zn^0$ stripping/plating occurs on the anode (**Fig. 6a**). **Fig. 6b** displays the CV curves of the NiCoP/$NiCo_2S_4$//Zn battery at various scan rates. Well-defined symmetric redox peaks can still be observed even at the high scan rate of 60 mV s^{-1}, revealing the highly reversible redox reaction. As shown in the charge-discharge curves of **Fig. 6c**, the discharge plateau of NiCoP/$NiCo_2S_4$//Zn battery is approximately at 1.7 V. Additionally, the NiCoP/$NiCo_2S_4$//Zn battery shows better performances than $NiCo_2S_4$//Zn battery (**Fig. S8**). Particularly, the NiCoP/$NiCo_2S_4$//Zn battery exhibits much higher specific capacity than that of $NiCo_2S_4$//Zn battery, which is clearly demonstrated by comparison CV and discharge curves (**Fig. S9**). Notably, the NiCoP/$NiCo_2S_4$//Zn battery yields an incredibly high specific capacity of 265.1 mA h g^{-1} at a high current density of 5 A g^{-1} (**Fig. 6d**), which are substantially better than that of the $NiCo_2S_4$//Zn battery (144.3 mA h g^{-1}) and most reported Zn-ion batteries, such as $Ni(OH)_2$/CNFs//Zn (184 mA h g^{-1} at 5 mA cm^{-2}),[46] Co_3O_4//Zn (162 mA h g^{-1} at 1 A g^{-1}) [47], Ni_3S_2//Zn (148 mA h g^{-1} at 0.2 A g^{-1})[48], NiO//ZnO (203 mA h g^{-1} at 0.5 mA cm^{-2}) [14], $NiCo_2O_4$//Zn (183.1 mA h g^{-1} at 1.6 A g^{-1}) [45], Zn//R-Co_3O_4(240.8 mA h g^{-1} at 2 mA cm^{-2}) [18]. The NiCoP/$NiCo_2S_4$//Zn battery have a specific capacity of 139.7 mA h g^{-1} with ~ 53% capacity retention at 10 A g^{-1}, indicating its excellent rate capability. The high rate capability of the NiCoP/$NiCo_2S_4$//Zn battery is further demonstrated in **Fig. 6e**, where the current density is increased from 5 to 10 A g^{-1} and returned to 5 A g^{-1}. The NiCoP/$NiCo_2S_4$//Zn battery delivers an average capacity of 264.9, 242.1, 206.2, 175.8,

155.2, and 139.7 mA h g^{-1} at 5, 6, 7, 8, 9, 10 A g^{-1}, respectively. When the current density is reduced back to 5 A g^{-1} after 50 cycles, the average capacity of 274.4 mA h g^{-1} is recovered, revealing excellent rate performance. **Fig. 6f** shows the long-term cycling performance of the NiCoP/$NiCo_2S_4$//Zn battery collected at a high scan rate of 100 mV s^{-1}. The NiCoP/$NiCo_2S_4$//Zn battery maintains 96.9% of the initial capacity after 5000 cycles. The NiCoP/$NiCo_2S_4$ nanosheet arrays are well-reserved, inserted in **Fig. 6f**, further demonstrating the excellent cycling performance.

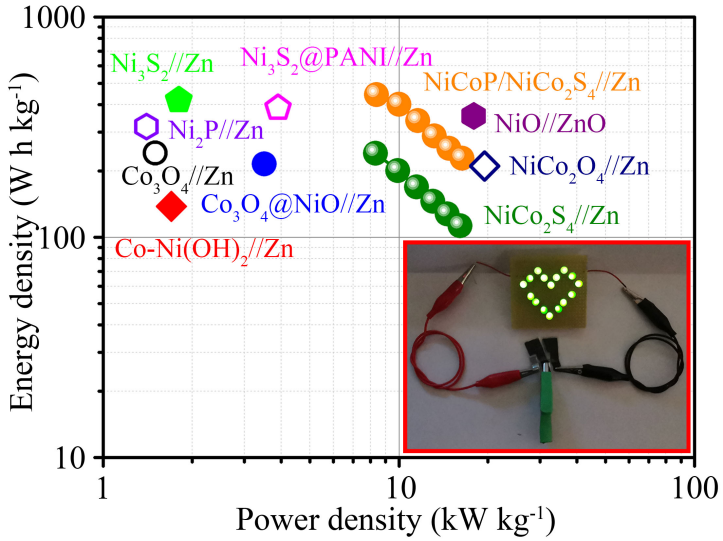

Fig. 7 Ragone plots of $NiCo_2S_4$//Zn battery and NiCoP/$NiCo_2S_4$//Zn battery compared with other similar works. The inset is the digital photo of heart-shaped LEDs powered by two as-fabricated NiCoP/$NiCo_2S_4$//Zn batteries in series.

Energy density and power density are two important parameters to estimate the practicability of energy storage devices. **Fig. 7** shows the Ragone plots of as-assembled $NiCo_2S_4$//Zn battery and NiCoP/$NiCo_2S_4$//Zn battery. It could be observed that the NiCoP/$NiCo_2S_4$//Zn battery delivers a maximum energy density of

444.7 W h kg^{-1} at the power density of 8.4 kW kg^{-1}. When the power density is increased to 16.3 kW kg^{-1}, the energy density still remains 228.2 W h kg^{-1}. While the $NiCo_2S_4$//Zn battery only delivers a maximum energy density of 240.5 W h kg^{-1} at the power density of 8.3 kW kg^{-1}. The energy density of the obtained NiCoP/$NiCo_2S_4$//Zn battery is close to or even better than some aqueous Zn-ion batteries reported previously, such as NiO//ZnO (355.7 W h kg^{-1} at 17.9 kW kg^{-1}) [14], Ni_2P//Zn (318.0 W h kg^{-1} at 1.4 kW kg^{-1}) [49], Ni_3S_2//Zn (419.6 W h kg^{-1} at 1.8 kW kg^{-1}) [48], Ni_3S_2@PANI//Zn (386.7 W h kg^{-1} at 3.9 kW kg^{-1})[44], Co_3O_4//Zn (241.0 W h kg^{-1} at 1.5 kW kg^{-1}) [47], Co_3O_4@NiO//Zn (215.5 W h kg^{-1} at 3.5 kW kg^{-1})[50], $NiCo_2O_4$//Zn (210.7 W h kg^{-1} at 19.5 kW kg^{-1}) [45], and Co-$Ni(OH)_2$//Zn (138.0 W h kg^{-1} at 1.7 kW kg^{-1}) [51]. The inset of **Fig.7** shows that two as-fabricated batteries connected in series can effectively power heart-shaped LEDs indicators, demonstrating the great promise for potential practical utilization.

4. Conclusion

In summary, we report the synthesis of heterostructured NiCoP/$NiCo_2S_4$ nanosheet arrays on carbon cloth through treating $NiCo_2S_4$ nanosheet arrays in the presence of P source and demonstrate its excellent property as the electrode material in aqueous Zn-ion batteries. The utilization of highly electrochemical activity between NiCoP and $NiCo_2S_4$ enables fast electron transport and rapid ion diffusion. As a result, the NiCoP/$NiCo_2S_4$ electrode shows a large specific capacity of 251.1 mA h g^{-1} at a high current density of 10 A g^{-1} and satisfactory rate capability (retaining about 76% even

at 50 A g^{-1}). Furthermore, the assembled NiCoP/$NiCo_2S_4$//Zn battery delivers a high specific capacity of 265.1 mA h g^{-1} at 5 A g^{-1}, excellent cycling stability with 96.9% retention after 5000 cycles, as well as a competitive energy density of 444.7 W h kg^{-1} at the power density of 8.4 kW kg^{-1}. The successful construction of aqueous Zn-ion batteries by interfacial engineering of electrode materials sheds light on the exploration of high-performance energy storage devices in the future.

Acknowledgements

This work was financially supported by the National Natural Science Foundation of China (Grant No. 51602049, 51708504), and China Postdoctoral Science Foundation (2017M610217 and 2018T110322).

References

[1] Y. Chen, W. Zhang, D. Zhou, H. Tian, D. Su, C. Wang, D. Stockdale, F. Kang, B. Li, G. Wang, Co-Fe Mixed Metal Phosphide Nanocubes with Highly Interconnected-Pore Architecture as an Efficient Polysulfide Mediator for Lithium-Sulfur Batteries, ACS Nano 13 (2019) 4731-4741.

[2] G.Z. Fang, J. Zhou, A.Q. Pan, S.Q. Liang, Recent Advances in Aqueous Zinc-Ion Batteries, ACS Energy Letters 3 (2018) 2480-2501.

[3] Y.N. Shen, Z.H. Li, Z. Cui, K. Zhang, R.J. Zou, F. Yang, K.B. Xu, Boosting the interface reaction activity and kinetics of cobalt molybdate by phosphating treatment for aqueous zinc-ion batteries with high energy density and long cycle life, Journal of Materials Chemistry A 8 (2020) 21044-21052.

[4] J. Liu, J. Wang, Z. Ku, H. Wang, S. Chen, L. Zhang, J. Lin, Z.X. Shen, Aqueous Rechargeable Alkaline CoxNi2-xS2/TiO2 Battery, ACS Nano 10 (2016) 1007-1016.

[5] B.Y. Tang, L.T. Shan, S.Q. Liang, J. Zhou, Issues and opportunities facing aqueous zinc-ion batteries, Energy & Environmental Science 12 (2019) 3288-3304.

[6] K. Zhang, X. Ye, Y. Shen, Z. Cen, K. Xu, F. Yang, Interface engineering of Co3O4 nanowire arrays with ultrafine NiO nanowires for high-performance rechargeable alkaline batteries, Dalton transactions 49 (2020) 8582-8590.

[7] M. Huang, M. Li, C.J. Niu, Q. Li, L.Q. Mai, Recent Advances in Rational Electrode Designs for High-Performance Alkaline Rechargeable Batteries, Advanced Functional Materials 29 (2019) 1807847.

[8] S.W. Zhang, B.S. Yin, Y.Z. Luo, L. Shen, B.S. Tang, Z.K. Kou, X.X. Liu, D.B.K. Lim, D.M. Gu, Z.B. Wang, H. Gong, Fabrication and theoretical investigation of cobaltosic sulfide nanosheets for flexible aqueous Zn/Co batteries, Nano Energy 68 (2020) 104314.

[9] J. Liu, M. Chen, L. Zhang, J. Jiang, J. Yan, Y. Huang, J. Lin, H.J. Fan, Z.X. Shen, A flexible alkaline rechargeable Ni/Fe battery based on graphene foam/carbon nanotubes hybrid film, Nano letters 14 (2014) 7180-7187.

[10] Y. Jiao, W. Hong, P. Li, L. Wang, G. Chen, Metal-organic framework derived Ni/NiO micro-particles with subtle lattice distortions for high-performance electrocatalyst and supercapacitor, Applied Catalysis B: Environmental 244 (2019) 732-739.

[11] H. Kim, G. Jeong, Y.U. Kim, J.H. Kim, C.M. Park, H.J. Sohn, Metallic anodes for next generation secondary batteries, Chemical Society reviews 42 (2013) 9011-9034.

[12] F. Liu, Z.X. Chen, G.Z. Fang, Z.Q. Wang, Y.S. Cai, B.Y. Tang, J. Zhou, S.Q. Liang, V2O5 Nanospheres with Mixed Vanadium Valences as High Electrochemically Active Aqueous Zinc-Ion Battery Cathode, Nano-Micro Letters 11 (2019) 25.

[13] P. Hu, T. Wang, J. Zhao, C. Zhang, J. Ma, H. Du, X. Wang, G. Cui, Ultrafast Alkaline Ni/Zn Battery Based on Ni-Foam-Supported Ni3S2 Nanosheets, ACS applied materials & interfaces 7 (2015) 26396-26399.

[14] J. Liu, C. Guan, C. Zhou, Z. Fan, Q. Ke, G. Zhang, C. Liu, J. Wang, A Flexible Quasi-Solid-State Nickel-Zinc Battery with High Energy and Power Densities Based

on 3D Electrode Design, Advanced Materials 28 (2016) 8732-8739.

[15] Y. Zeng, Y. Meng, Z. Lai, X. Zhang, M. Yu, P. Fang, M. Wu, Y. Tong, X. Lu, An Ultrastable and High-Performance Flexible Fiber-Shaped Ni-Zn Battery based on a Ni-NiO Heterostructured Nanosheet Cathode, Advanced Materials 29 (2017) 1702698.

[16] Y. Tang, X. Li, H. Lv, D. Xie, W. Wang, C. Zhi, H. Li, Stabilized Co 3+ /Co 4+ Redox Pair in In Situ Produced CoSe 2− x Derived Cobalt Oxides for Alkaline Zn Batteries with 10 000-Cycle Lifespan and 1.9-V Voltage Plateau, Advanced Energy Materials 10 (2020) 2000892.

[17] M. Gong, Y.G. Li, H.B. Zhang, B. Zhang, W. Zhou, J. Feng, H.L. Wang, Y.Y. Liang, Z.J. Fan, J. Liu, H.J. Dai, Ultrafast high-capacity NiZn battery with NiAlCo-layered double hydroxide, Energy & Environmental Science 7 (2014) 2025-2032.

[18] Y.Z. Lu, J. Wang, S.Q. Zeng, L.J. Zhou, W. Xu, D.Z. Zheng, J. Liu, Y.X. Zeng, X.H. Lu, An ultrathin defect-rich Co3O4 nanosheet cathode for high-energy and durable aqueous zinc ion batteries, Journal of Materials Chemistry A 7 (2019) 21678-21683.

[19] V. Caldeira, R. Rouget, F. Fourgeot, J. Thiel, F. Lacoste, L. Dubau, M. Chatenet, Controlling the shape change and dendritic growth in Zn negative electrodes for application in Zn/Ni batteries, Journal of Power Sources 350 (2017) 109-116.

[20] Y.N. Shen, K. Zhang, F. Yang, Z.H. Li, Z. Cui, R.J. Zou, Q. Liu, J.Q. Hu, K.B. Xu, Oxygen vacancies-rich cobalt-doped NiMoO4 nanosheets for high energy density and stable aqueous Ni-Zn battery, SCIENCE CHINA Materials 63 (2020) 1205-1215.

[21] J. Xiao, L. Wan, S. Yang, F. Xiao, S. Wang, Design hierarchical electrodes with highly conductive NiCo2S4 nanotube arrays grown on carbon fiber paper for high-performance pseudocapacitors, Nano letters 14 (2014) 831-838.

[22] L. Shen, L. Yu, H.B. Wu, X.Y. Yu, X. Zhang, X.W. Lou, Formation of nickel cobalt sulfide ball-in-ball hollow spheres with enhanced electrochemical pseudocapacitive properties, Nature communications 6 (2015) 6694.

[23] B.Y. Guan, L. Yu, X. Wang, S. Song, X.W. Lou, Formation of Onion-Like NiCo2

S4 Particles via Sequential Ion-Exchange for Hybrid Supercapacitors, Advanced Materials 29 (2017) 1605051.

[24] W. Zeng, G. Zhang, X. Wu, K. Zhang, H. Zhang, S. Hou, C. Li, T. Wang, H. Duan, Construction of hierarchical CoS nanowire@NiCo2S4 nanosheet arrays via one-step ion exchange for high-performance supercapacitors, Journal of Materials Chemistry A 3 (2015) 24033-24040.

[25] H. Anwer, H. Lee, H.-R. Kim, H.-K. Kim, J.-W. Park, Selective transport and separation of charge–carriers by an electron transport layer in NiCo2S4/CdO@CC for excellent water splitting, Applied Catalysis B: Environmental 265 (2020).

[26] X. Chen, D. Chen, X. Guo, R. Wang, H. Zhang, Facile Growth of Caterpillar-like NiCo2S4 Nanocrystal Arrays on Nickle Foam for High-Performance Supercapacitors, ACS applied materials & interfaces 9 (2017) 18774-18781.

[27] Y. Shen, K. Zhang, B. Chen, F. Yang, K. Xu, X. Lu, Enhancing the electrochemical performance of nickel cobalt sulfides hollow nanospheres by structural modulation for asymmetric supercapacitors, Journal of Colloid and Interface Science 557 (2019) 135-143.

[28] C.P. Han, T.F. Zhang, J.Q. Li, B.H. Li, Z.Q. Lin, Enabling flexible solid-state Zn batteries via tailoring sulfur deficiency in bimetallic sulfide nanotube arrays, Nano Energy 77 (2020) 105165.

[29] J. Huang, Y. Xiong, Z. Peng, L. Chen, L. Wang, Y. Xu, L. Tan, K. Yuan, Y. Chen, A General Electrodeposition Strategy for Fabricating Ultrathin Nickel Cobalt Phosphate Nanosheets with Ultrahigh Capacity and Rate Performance, ACS Nano 14 (2020) 14201-14211.

[30] H. Liang, A.N. Gandi, D.H. Anjum, X. Wang, U. Schwingenschlogl, H.N. Alshareef, Plasma-Assisted Synthesis of NiCoP for Efficient Overall Water Splitting, Nano letters 16 (2016) 7718-7725.

[31] T.T. Nguyen, J. Balamurugan, N.H. Kim, J.H. Lee, Hierarchical 3D Zn–Ni–P nanosheet arrays as an advanced electrode for high-performance all-solid-state asymmetric supercapacitors, Journal of Materials Chemistry A 6 (2018) 8669-8681.

[32] J. Tian, Q. Liu, A.M. Asiri, X. Sun, Self-supported nanoporous cobalt phosphide

nanowire arrays: an efficient 3D hydrogen-evolving cathode over the wide range of pH 0-14, Journal of the American Chemical Society 136 (2014) 7587-7590.

[33] W. Song, J. Wu, G. Wang, S. Tang, G. Chen, M. Cui, X. Meng, Rich-Mixed-Valence Ni x Co 3−x P y Porous Nanowires Interwelded Junction-Free 3D Network Architectures for Ultrahigh Areal Energy Density Supercapacitors, Advanced Functional Materials 28 (2018) 1804620.

[34] N. Zhang, Y. Li, J. Xu, J. Li, B. Wei, Y. Ding, I. Amorim, R. Thomas, S.M. Thalluri, Y. Liu, G. Yu, L. Liu, High-Performance Flexible Solid-State Asymmetric Supercapacitors Based on Bimetallic Transition Metal Phosphide Nanocrystals, ACS Nano 13 (2019) 10612-10621.

[35] Y. Li, X. Tan, H. Tan, H. Ren, S. Chen, W. Yang, S.C. Smith, C. Zhao, Phosphine vapor-assisted construction of heterostructured Ni2P/NiTe2 catalysts for efficient hydrogen evolution, Energy & Environmental Science 13 (2020) 1799-1807.

[36] Y. Zeng, Z. Lai, Y. Han, H. Zhang, S. Xie, X. Lu, Oxygen-Vacancy and Surface Modulation of Ultrathin Nickel Cobaltite Nanosheets as a High-Energy Cathode for Advanced Zn-Ion Batteries, Advanced Materials 30 (2018) 1802396.

[37] W. Chu, Z. Shi, Y. Hou, D. Ma, X. Bai, Y. Gao, N. Yang, Trifunctional of Phosphorus-Doped NiCo2O4 Nanowire Materials for Asymmetric Supercapacitor, Oxygen Evolution Reaction, and Hydrogen Evolution Reaction, ACS Applied Materials & Interfaces 12 (2020) 2763-2772.

[38] S.C. Tang, B.G. Zhu, X.L. Shi, J. Wu, X.K. Meng, General Controlled Sulfidation toward Achieving Novel Nanosheet-Built Porous Square-FeCo2S4-Tube Arrays for High-Performance Asymmetric All-Solid-State Pseudocapacitors, Advanced Energy Materials 7 (2017) 1601985.

[39] Y. Wang, Z. Chen, T. Lei, Y. Ai, Z. Peng, X. Yan, H. Li, J. Zhang, Z.M. Wang, Y.-L. Chueh, Hollow NiCo2S4 Nanospheres Hybridized with 3D Hierarchical Porous rGO/Fe2O3 Composites toward High-Performance Energy Storage Device, Advanced Energy Materials 8 (2018) 1703453.

[40] B. Guan, Y. Li, B.Y. Yin, K.F. Liu, D.W. Wang, H.H. Zhang, C.J. Cheng, Synthesis of hierarchical NiS microflowers for high performance asymmetric

supercapacitor, Chemical Engineering Journal 308 (2017) 1165-1173.
[41] C. Ye, L. Zhang, C.X. Guo, D.D. Li, A. Vasileff, H.H. Wang, S.Z. Qiao, A 3D Hybrid of Chemically Coupled Nickel Sulfide and Hollow Carbon Spheres for High Performance Lithium-Sulfur Batteries, Advanced Functional Materials 27 (2017) 1702524.
[42] H.C. Chen, S.P. Jiang, B.H. Xu, C.H. Huang, Y.Z. Hu, Y.L. Qin, M.X. He, H.J. Cao, Sea-urchin-like nickel-cobalt phosphide/phosphate composites as advanced battery materials for hybrid supercapacitors, Journal of Materials Chemistry A 7 (2019) 6241-6249.
[43] S. Li, N. Yang, L. Liao, Y. Luo, S. Wang, F. Cao, W. Zhou, D. Huang, H. Chen, Doping beta-CoMoO4 Nanoplates with Phosphorus for Efficient Hydrogen Evolution Reaction in Alkaline Media, ACS Applied Materials & Interfaces 10 (2018) 37038-37045.
[44] L.J. Zhou, X.Y. Zhang, D.Z. Zheng, W. Xu, J. Liu, X.H. Lu, Ni3S2@PANI core-shell nanosheets as a durable and high-energy binder-free cathode for aqueous rechargeable nickel-zinc batteries, Journal of Materials Chemistry A 7 (2019) 10629-10635.
[45] H. Zhang, X. Zhang, H. Li, Y. Zhang, Y. Zeng, Y. Tong, P. Zhang, X. Lu, Flexible rechargeable Ni//Zn battery based on self-supported NiCo2O4 nanosheets with high power density and good cycling stability, Green Energy & Environment 3 (2018) 56-62.
[46] Y. Jian, D.M. Wang, M.Z. Huang, H.L. Jia, J.H. Sun, X.K. Song, M.Y. Guan, Facile Synthesis of Ni(OH)(2)/Carbon Nanofiber Composites for Improving NiZn Battery Cycling Life, ACS Sustainable Chemistry & Engineering 5 (2017) 6827-6834.
[47] X. Wang, F. Wang, L. Wang, M. Li, Y. Wang, B. Chen, Y. Zhu, L. Fu, L. Zha, L. Zhang, Y. Wu, W. Huang, An Aqueous Rechargeable Zn//Co3 O4 Battery with High Energy Density and Good Cycling Behavior, Advanced Materials 28 (2016) 4904-4911.
[48] Y. He, P. Zhang, H. Huang, X. Li, X. Zhai, B. Chen, Z. Guo, Engineering Sulfur Vacancies of Ni3S2 Nanosheets as a Binder-Free Cathode for an Aqueous

Rechargeable Ni-Zn Battery, ACS Applied Energy Materials 3 (2020) 3863-3875.
[49] J. Wen, Z. Feng, H. Liu, T. Chen, Y. Yang, S. Li, S. Sheng, G. Fang, In-situ synthesized Ni2P nanosheet arrays as the cathode for novel alkaline Ni//Zn rechargeable battery, Applied Surface Science 485 (2019) 462-467.
[50] Z.Y. Lu, X.C. Wu, X.D. Lei, Y.P. Li, X.M. Sun, Hierarchical nanoarray materials for advanced nickel-zinc batteries, Inorganic Chemistry Frontiers 2 (2015) 184-187.
[51] C. Xu, J. Liao, C. Yang, R.Z. Wang, D. Wu, P.C. Zou, Z.Y. Lin, B.H. Li, F.Y. Kang, C.P. Wong, An ultrafast, high capacity and superior longevity Ni/Zn battery constructed on nickel nanowire array film, Nano Energy 30 (2016) 900-908.